

# Mechanical Regulation Triboelectric Nanogenerator with Controllable Output Performance for Random Energy Harvesting

Mengfei Yin, Xiaohui Lu, Guangda Qiao, Yuhong Xu, Yuqi Wang, Tinghai Cheng,\*  
and Zhong Lin Wang\*

Recycling of random mechanical energy in the environment has become an important research hotspot. The triboelectric nanogenerators (TENGs) were invented to harvest energy, and have been widely applied due to their simple structure, small size, and low cost. This paper reports a mechanical regulation triboelectric nanogenerator (MR-TENG) for the first time with controllable output performance used to harvest random or irregular energy in the environment. It comprises a transmission unit, switch structure, generator unit, flywheel, and shell. Random linear motion or rocking motion is transferred via the transmission unit to the flywheel. The rotor of the generator unit fixed on the flywheel and the stator of the generator unit fixed on the shell combine. By controlling the storage and release of energy in the flywheel, the switch structure assists the flywheel to convert random or irregular energy into a controllable and stable energy output. The MR-TENG can generate an open-circuit voltage of 350 V, a short-circuit current of 12  $\mu$ A, a transfer charge of 130 nC, and a peak power of 2.52 mW. Furthermore, a thermometer and more than 300 light emitting diodes (LEDs) are separately powered by this MR-TENG in simulated water waves, demonstrating its potential application in water wave energy harvesting.

## 1. Introduction

With the intensification of the energy crisis and global warming, the recycling of mechanical energy in the environment has become an important topic of research in the field

M. Yin, G. Qiao, Y. Xu, Y. Wang, Prof. T. Cheng, Prof. Z. L. Wang  
Beijing Institute of Nanoenergy and Nanosystems  
Chinese Academy of Sciences  
Beijing 100083, China  
E-mail: chengtinghai@binn.cas.cn; zhong.wang@mse.gatech.edu

M. Yin, Dr. X. Lu, G. Qiao, Y. Xu, Y. Wang, Prof. T. Cheng  
School of Mechatronic Engineering  
Changchun University of Technology  
Changchun, Jilin 130012, China

Prof. Z. L. Wang  
School of Materials Science and Engineering  
Georgia Institute of Technology  
Atlanta, GA 30332-0245, USA

 The ORCID identification number(s) for the author(s) of this article can be found under <https://doi.org/10.1002/aenm.202000627>.

DOI: 10.1002/aenm.202000627

of energy collection.<sup>[1–5]</sup> However, ambient mechanical energy is characterized as having a wide range of operating frequencies, low amplitudes, randomness, and irregularity.<sup>[6–8]</sup> This sets a barrier for the mechanical energy collection for electromagnetic generators with weak performance in power generation at low frequencies.<sup>[9,10]</sup> In 2012, triboelectric nanogenerators (TENGs) with high power density, high energy conversion efficiency, and low costs were proposed by Wang's group,<sup>[11]</sup> which aroused comprehensive attention on the aspect of energy harvesting research.<sup>[12–17]</sup>

Based on the coupling of triboelectrification effect and electrostatic induction, TENGs show excellent characteristics at low frequency and low amplitude, so they can convert ambient mechanical energy into electrical energy efficiently.<sup>[18–24]</sup> Researchers have investigated harvesting energy from the ocean, human motion, and vibration and wind in the environment.<sup>[25–28]</sup> Depending on its operating

principle, the output characteristics of TENGs, especially the current, are determined by the external excitation.<sup>[29–32]</sup> However, the randomness and irregularity of energy from the environment results in an output performance of TENGs that is usually irregular and uncontrollable.<sup>[33,34]</sup> This has become one of the key problems restricting their applications.

In the paper, the research philosophy of a mechanical regulation triboelectric nanogenerator (MR-TENG) with controllable output performance for harvesting random energy is proposed for the first time. Through the combination of the energy storage structure and the control switch structure, the controllable output of TENG under random excitation is achieved. The MR-TENG is made up of five main components: transmission unit, switch structure, generator unit which includes stator and rotor, flywheel, and shell. The structural transmission unit transfers random linear or rocking motions in the environment to the flywheel. The rotor of the generator unit fixed on the flywheel includes six flexible blades and a thin-walled cylinder. The stator of the generator unit includes a shell with 12 copper electrodes pasted equidistant on the inner wall of this shell. The rotor and stator cooperate to convert rotational kinetic

energy into electrical energy. By adjusting the energy storage angle of the switch structure, energy harvesting and energy release by the MR-TENG can be controlled enabling it to convert random or irregular energy in the environment into a controllable energy output. Moreover, if the energy storage angle of the switch structure is set, a stable output from MR-TENG is achieved through the cooperation of the switch structure and the flywheel. Experimental results depict that the MR-TENG can exhibit an open-circuit voltage of 350 V, a short-circuit current of 12  $\mu$ A, a transfer charge of 130 nC, and a peak power of 2.52 mW when operating under random or irregular excitation conditions. Furthermore, an experiment was conducted with the MR-TENG in simulated water waves showing its potential applications by separately powering 375 LEDs and a thermometer.

## 2. Result and Discussion

### 2.1. Structure and Operation Principle of the MR-TENG

The structure of the MR-TENG (Figure 1a) features a switching device for controlling energy storage time (Figure 1b) and a generator unit and flywheel (Figure 1c). The fabricated device (Figure 1d) has five main parts: transmission unit, switch structure, generator unit, flywheel, and shell. The transmission unit is used to convert the external linear motion into a rocking motion required by the generator unit. The switch structure combines with the flywheel to control the energy storage and the energy release in converting the external irregular linear motion into regular rotational motion. Figure 1e shows the switch disc. The generator unit consists of a rotor and a stator (Figure 1f).

Step-by-step details of the movement of the MR-TENG are illustrated to show the operating principle (Figure 2a and Figure S1, Supporting Information). In the initial state of

power generation, there is no external excitation input to the MR-TENG (Figure 2a(i)). The transmission unit is at a standstill, the switch structure is unlocked, and the spiral spring is not compressed. Therefore, the generator unit is not rotating and no electrical signal is outputted. When an external excitation moves the rack, the spring compresses (Figure 2a(ii)) and a one-way clutch drives the switch disc to rotate counter-clockwise via the shaft system. At this instant, the switch disc pushes the limit rod to lock the flywheel. And the spiral spring can be compressed to the maximum extent to store energy. The rack then moves in the reverse direction as the spring relaxes (Figure 2a(iii)). The one-way clutch rotates clockwise but does not provide any reverse torque to the shaft. This switch structure is still in the locked state, and no electrical signal is outputted from the generator unit. After several excitation cycles, the limit rod returns to the initial position with the assistance of a reset spring. The kinetic energy of flywheel is transformed from the elastic potential energy stored by the spiral spring which is converted into electrical energy with help of the power generating unit. (Figure 2a(iv)).

The operating principle of the MR-TENG is shown in Figure 2b,c, which is based on the coupling of triboelectrification effect and electrostatic induction. The flexible blades (i.e., tribonegative material) made by fluorinated ethylene propylene (FEP) slide between two adjacent electrodes  $A_1$  and  $A_2$ . To better explain operating principle of the generator unit, the sliding of the blade from  $A_1$  to  $A_2$  is described in steps (Figure 2b). In the initial state when the blade overlaps electrode  $A_1$  (Figure 2b(i)), it receives a negative induced charge through triboelectrification, whereas  $A_1$  and  $A_2$  become positively charge. Then, as the blade slides from  $A_1$  to  $A_2$ , the electrostatic balance is broken and a potential difference appears between  $A_1$  and  $A_2$  (Figure 2b(ii)). The negative charges on  $A_1$  are transferred to  $A_2$  through the external circuit to rebalance the electrostatic state under electrostatic induction, until it reaches the third state when the blade overlaps  $A_2$  (Figure 2b(iii)). As the rotor

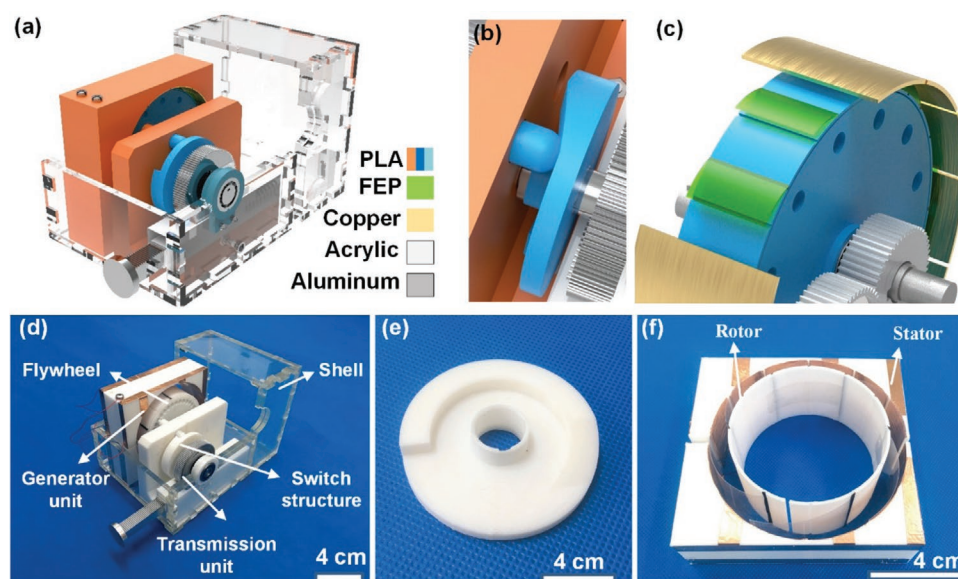


**Figure 1.** Basic structural of the MR-TENG: a) schematic description of the assembly, b) switch structure, c) generator unit and flywheel; photos of d) the whole structure, e) switch disc, and f) rotor structure of the generator unit.

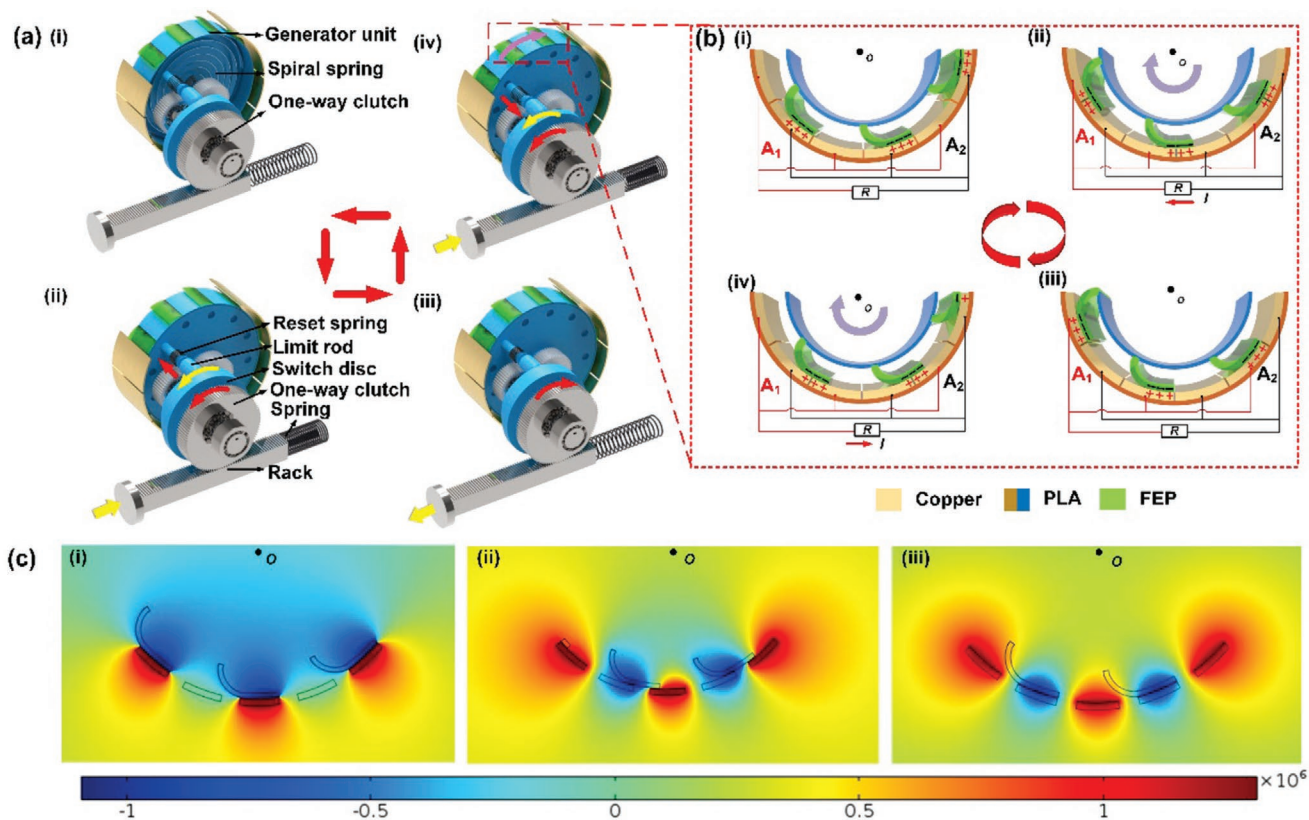


**Figure 2.** Operation principle of the MR-TENG: a) different states of motion transmission unit, b) schematic of the operating principle for the rotor and stator, and c) simulation of the electrostatic field distribution for three states of the flywheel.

structure of the generator unit continues rotating, the negative charges on  $A_2$  transfer to  $A_1$  through the external circuit (Figure 2b(iv)). To verify the feasibility of these states of the generator unit, a field analysis was performed of these states using COMSOL Multiphysics software employing on finite-element methods (Figure 2c).

## 2.2. Performance

For the sake of making the output characteristic of the MR-TENG reach the excellent value, different lengths of the blades, flywheel masses, and spiral spring stiffnesses were studied under fixed excitation conditions. The excitation amplitude is 4 mm and frequency is 2 Hz (Figure 3 and Figure S2, Supporting Information). Figure 3g shows that, as the blade length increases, the rotor running time gradually decreases over a single cycle. This is because the friction between blade and electrode on the stator raise with the increase of the length of blade, which hinders the rotor operation.<sup>[35]</sup> The output energy displays a normal distribution as blade length increases with an energy peak just as the length of blade is 55 mm.

To understand the output characteristics of masses and spiral spring stiffness, the open-voltage and short-circuit current were measured in experiments with several spiral springs of different stiffnesses and flywheels of different masses.

The stiffness  $k$  of each spring was obtained using (Table S1, Supporting Information)<sup>[36]</sup>

$$k = \frac{T}{\varphi} = \frac{E_m I_m}{l_m} \quad (1)$$

where  $T$  and  $\varphi$  denote the torque and corner of the spiral spring,  $E_m$  and  $l_m$  represent the elastic modulus and the working length of the spring steel. The moment of inertia  $I_m$  is obtained using

$$I_m = \frac{b_m h_m^3}{12} \quad (2)$$

where  $b_m$  denotes the width of the spiral spring and  $h_m$  thickness.

The output energy increases as the spiral spring stiffness increases (Figure 3i). For the same spiral spring stiffness, the relationship between running time and output performance on flywheel mass increased and decrease, respectively (Figure 3h). Moreover, as the flywheel mass increases, the open-circuit voltage (Figure 3, top row) and the charge transferred (Figure S3, Supporting Information) remained unchanged, whereas the short-circuit current decreased (Figure 3, middle row). By comparison, when the flywheel mass is 0.252 kg and the spring stiffness is 5.32 N mm rad<sup>-1</sup> the MR-TENG produced a high output performance (Figure 3h,i).

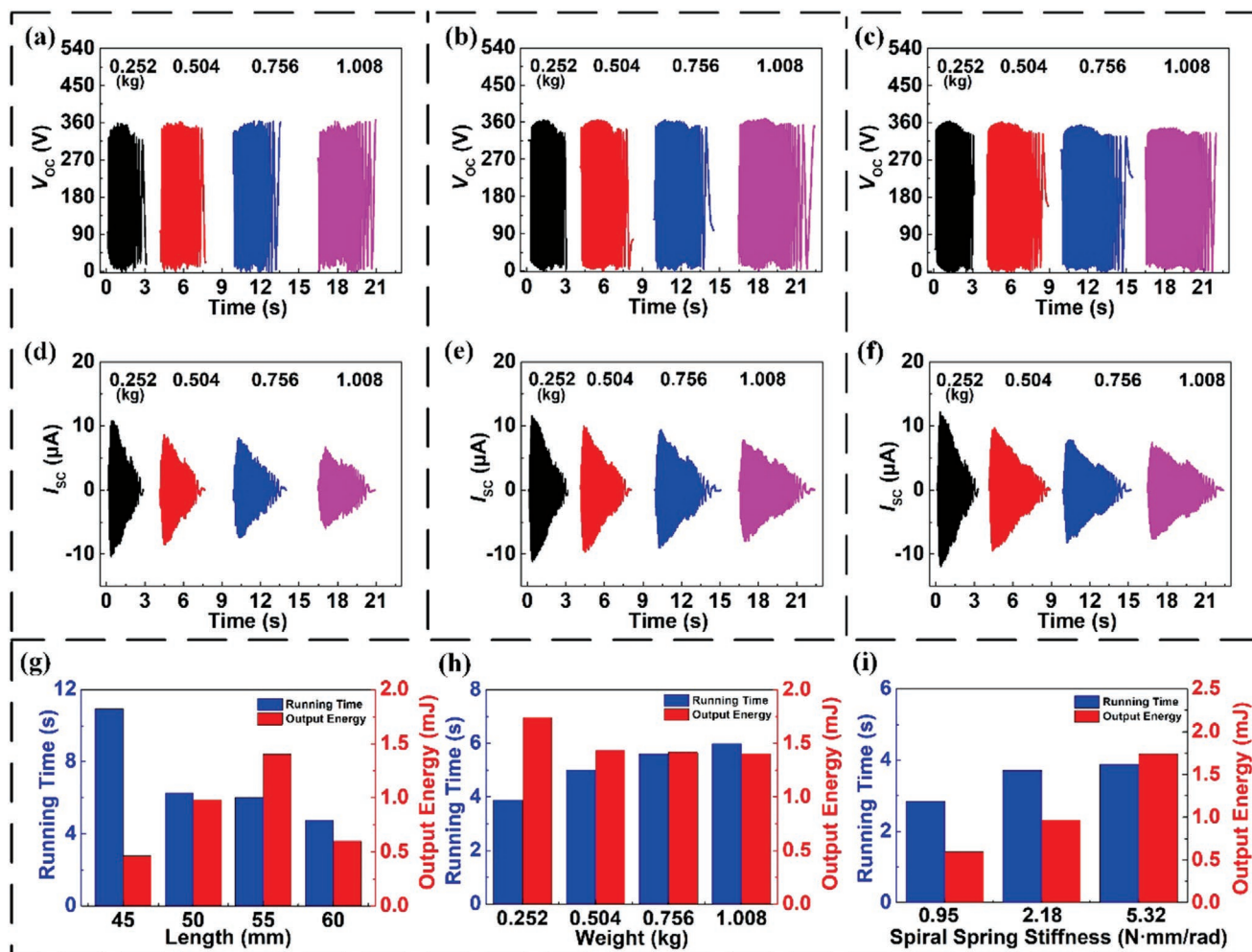


**Figure 3.** Demonstration of electrical output of the MR-TENG with various spiral spring stiffnesses and flywheel masses: (top row) open-circuit voltage and (middle row) short-circuit current response to the spiral spring stiffness of a,d) 0.95 N, b,e) 2.18, and c,f) 5.32 N mm rad<sup>-1</sup>. The relationship between running time and output performance on g) blade length, h) flywheel mass, and i) spiral spring stiffnesses.

The switch disc in the switch structure is the key structure of the MR-TENG. The energy storage angle  $\alpha$  (the angle of the projecting arc on the switch disc) is very important as it affects the energy storage effect of the spiral spring directly and subsequently the output performance (Movie S1, Supporting Information). **Figure 4** shows the output performance of different switching angles under the same excitation amplitude and different excitation frequencies. **Figure 4a,b** shows that the higher external excitation frequencies shorten the energy storage time significantly, but the open-circuit voltage, short-circuit current, and transferred charge remain unchanged when the energy storage angle is the same. Moreover, when the energy storage angle  $\alpha$  remains unchanged, the output performance does not change with changes in the external excitation frequency. With the same frequency and amplitude of the external excitation, the bigger energy storage angles extend the energy storage time and enhance the power generation performance of the MR-TENG. This is because a larger energy storage angle increases the amount of compression of the spiral spring, thereby increasing the stored energy and the corresponding energy released. The formula of the storage energy of the spiral spring  $U$  is

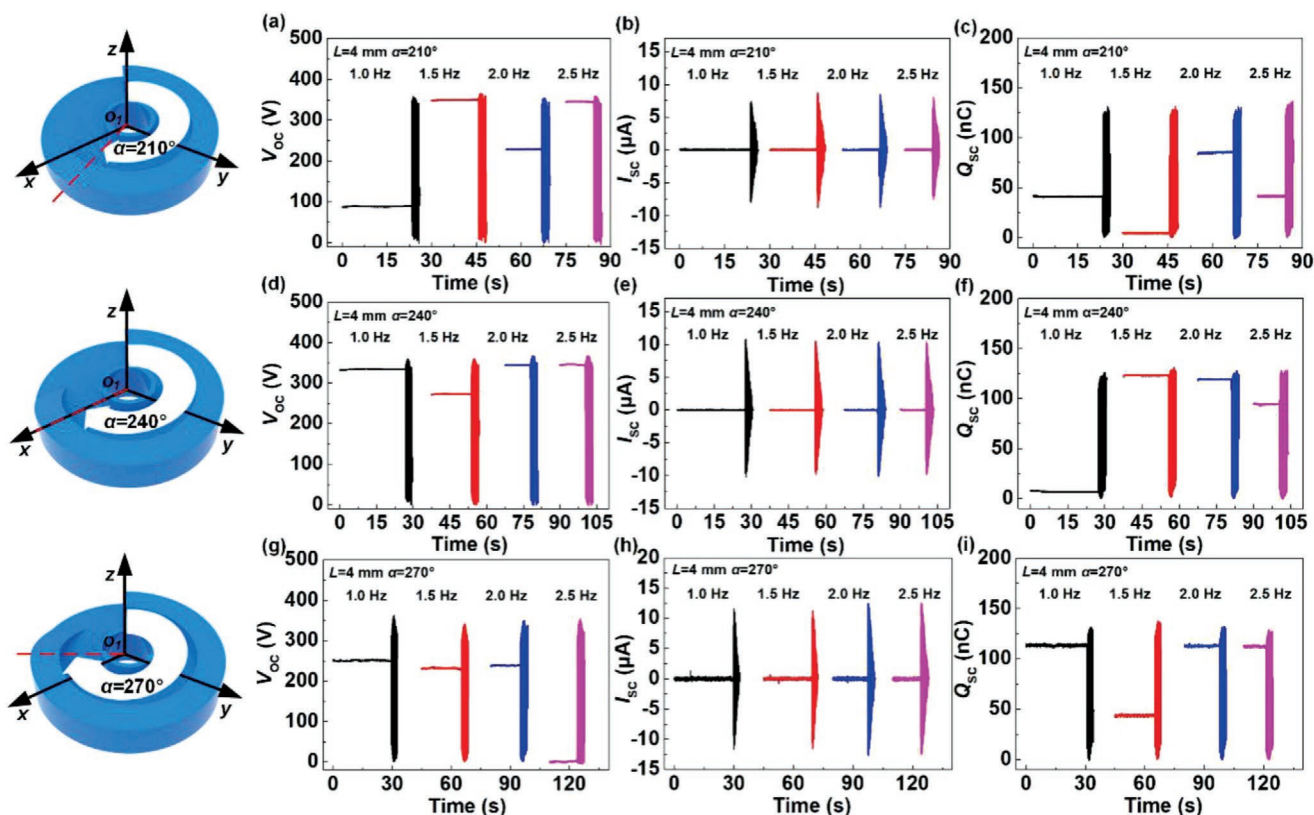
$$U = T\varphi \quad (3)$$

where  $T$  denotes the torque of the spiral spring, which may be regarded as linear in engineering calculations, and  $\varphi$  is the angle. Therefore, the energy of compression for the spiral spring  $U$  is quadratically related to  $\varphi$ . In this study,  $\varphi$  is denoted by

$$\varphi = \alpha \quad (4)$$

Therefore, the energy storage angle has an impact on the output performance of the MR-TENG.

Because the excitation amplitude of ambient external excitations is usually variable, the output characteristics under different excitation amplitudes were studied (**Figure 5**). In conjunction with **Figure 4g–i**, **Figure 5a–f** shows an analysis of the output performance for different excitation amplitudes and different excitation frequencies with the energy storage angle fixed at 270°. From this comparison, for the same excitation amplitude condition, the energy storage time decreases with increasing excitation frequency. The time for the release of energy is basically constant as is the output performance.



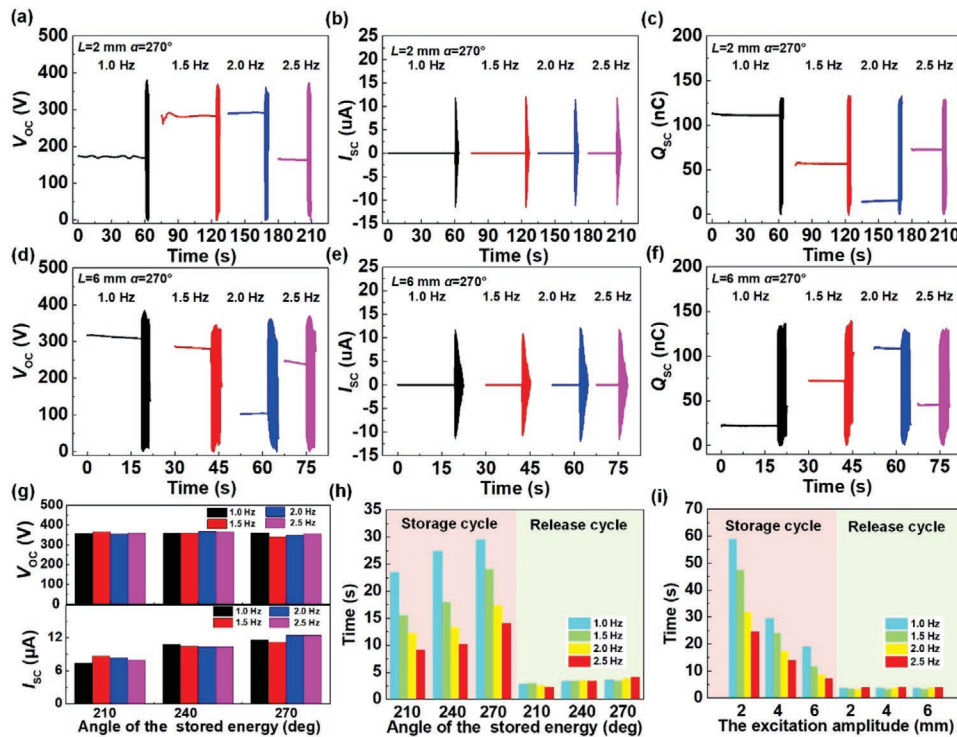
**Figure 4.** Output performance of the MR-TENG for a fixed excitation amplitude of 4 mm, different energy storage angles of the switching disc, and different excitation frequencies: open-circuit voltage, short-circuit current, and transferred charge when the angle of stored energy of the switching disc is (top row)  $210^\circ$ , (middle row)  $240^\circ$ , and (bottom row)  $270^\circ$ .

Figure 5g,h shows the effects of different energy storage angles on the output performance, energy storage time, and energy release time of the MR-TENG. As the energy storage angle increases, the open-circuit voltage does not change significantly, whereas the short-circuit current gradually increases. This is because as this angle increases, the energy stored in the spiral spring increases, allowing the flywheel to gain greater rotation speed when the energy is released. The rotation speed of the flywheel has an impact on the short-circuit current but has no effect on the open-circuit voltage. Hence, a larger energy storage angle will generate a larger short-circuit current. A larger switching angle also extends the energy storage time and energy release time. Under the same excitation frequency, the energy storage time decreases with increasing excitation amplitude; the time of energy release remains basically constant, and the output performance remains substantially constant (Figure 5i). Therefore, the output performance of the MR-TENG confirms that controllability is possible (Figure 5).

The output performances of the MR-TENG under simulated actual working conditions were also investigated, specifically, over four cycles, for different excitation amplitudes and fixed excitation frequency (Figure 6a–d), for different excitation frequencies with fixed excitation amplitude (Figure 6e–h), and different excitation amplitudes in multiple cycles (Figure 6i–l). Under different external excitation conditions, Figure 6a,e,i shows the measured displacement, Figure 6b,f,j shows the open-circuit voltage, Figure 6c,g,k shows the short-circuit

current, and Figure 6d,h,l shows open-circuit voltage and comparison of different cycles with different excitation conditions. Figure S4 (Supporting Information) shows the transferred charge of the MR-TENG with different excitation conditions. Evidently, under irregular external excitation conditions, the MR-TENG still produces the stable performance output.

The output performance analysis of the MR-TENG confirms that a stable output performance is possible even with random inputs (Figure 6i). Figure 7 shows the MR-TENG can charge different commercial capacitors with capacitances 4.7, 10, and 22  $\mu\text{F}$  to 10 V. Before changing the commercial capacitors, the MR-TENG was connected to a rectifier circuit. From the experimental data, the larger input frequency and larger excitation amplitude improve the charging efficiency. In addition, to better depict the output performance of the MR-TENG exerting various external loads, the voltage and current were also measured. From Figure 7b, when the resistance is low, the voltage of MR-TENG is low, but the current is high. When the resistance is raised gradually, the voltage of the MR-TENG rises but the current diminishes gradually. This is because the electric circuit is similar to a short-circuit scenario when the resistance is low and to an open-circuit situation when the resistance is high. From the peak power under different loads (Figure 7b), we see that the maximum peak power of MR-TENG is 2.52 mW. That is, the MR-TENG harvests random energy in the environment, Figure 7c presents a photo of the MR-TENG harvesting energy from water waves generated in a tank. The MR-TENG can power



**Figure 5.** Output performance of the MR-TENG with the stored energy angle of the switching disc fixed at  $270^\circ$ , and for different excitation amplitudes and excitation frequencies: a,d) open-circuit voltage, b,e) short-circuit current, and c,f) transfer charge when the excitation amplitudes is a–c) 2 mm and d–f) 6 mm; g) comparison of the open-circuit voltage and short-circuit current; h) output performance comparison of the energy storage cycle time and release cycle time at different angles and various excitation frequencies; i) as for (h) but for different excitation amplitudes.

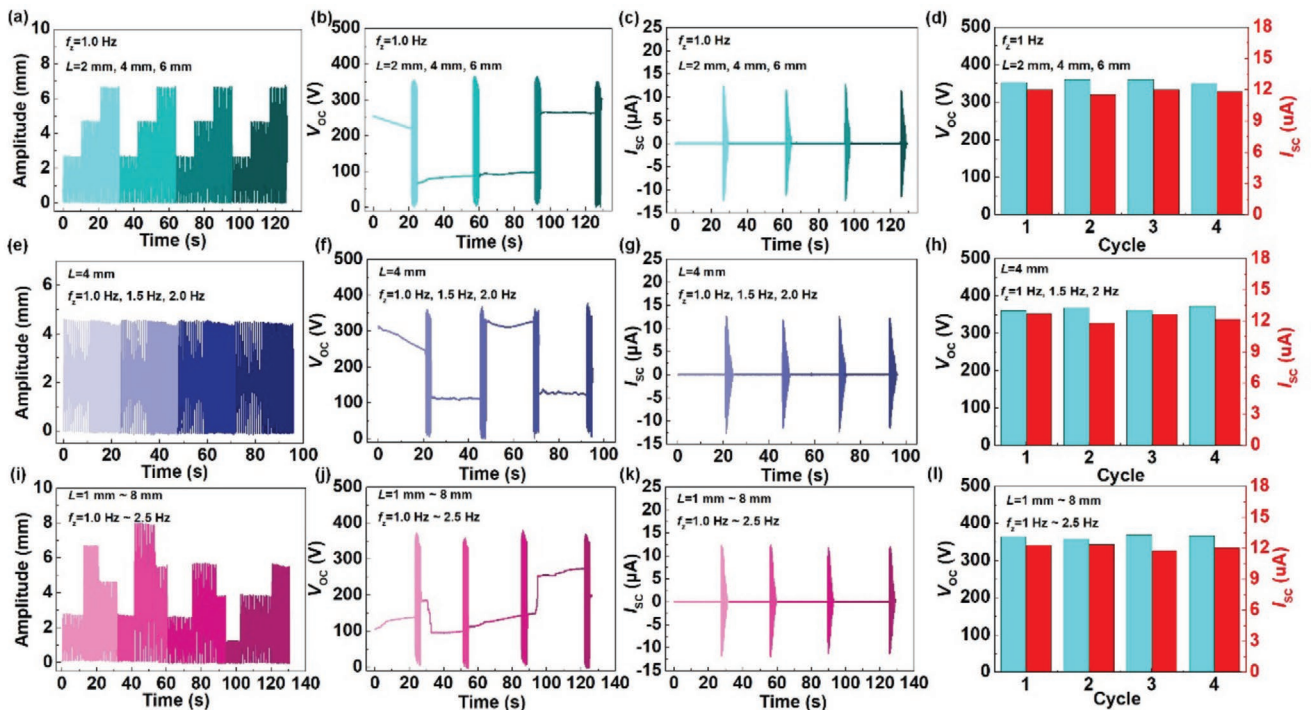


**Figure 6.** Output performance of the MR-TENG with various excitation conditions: a,e,i) excitation amplitude, b,f,j) open-circuit voltage, c,g,k) short-circuit current, and d,h,l) comparisons of different cycles when different excitation conditions have a–d) the same frequency and different amplitudes, e–h) same amplitude and different frequencies, and i–l) different amplitudes and frequencies.

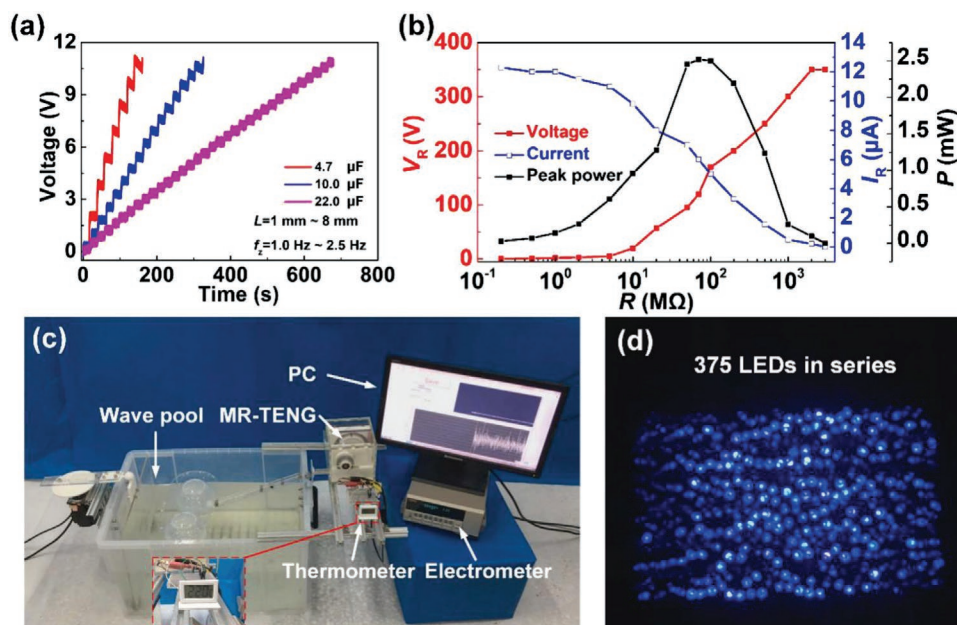


**Figure 7.** Demonstration of the MR-TENG for harvesting energy of random: a) voltage of different commercial capacitors during charging; b) voltage, current, and peak power output of MR-TENG under different external resistance loads; c) photo of the MR-TENG harvesting energy from water waves; d) photo of 375 LEDs being powered by a MR-TENG.

375 LEDs or a digital thermometer using rectifying circuit from harvested water wave energy (Movies S2 and S3, Supporting Information).

### 3. Conclusion

For capturing random mechanical energy in the environment efficiently, this study proposed and prototyped a MR-TENG. Comprising a transmission unit, a switch structure, a generator unit, a flywheel and a shell, this TENG has a controllable output performance. The switch structure and flywheel structure provides control of energy collection and subsequent release. Experiments have demonstrated that the MR-TENG converts random or irregular energy source into a controllable and stable energy output. From an analysis, a stable output performance was observed for an open-circuit voltage of 350 V, a short-circuit current of 12  $\mu\text{A}$ , a transfer charge of 130 nC, and a peak power of 2.52 mW. In addition, water wave experiments were performed to demonstrate its operating performance under ambient conditions. A thermometer and more than 300 LEDs (375 LEDs) were separately powered by the MR-TENG, demonstrating the potential application in energy harvesting of water waves. This study shows how to reduce the impact of the variability in external input on TENG making actual applications of TENGs more feasible.

### 4. Experimental Section

*Fabrication of the MR-TENG:* The MR-TENG mainly consists of transmission unit, switch structure, generator unit, flywheel, and shell.

The transmission unit consists of rack, gear, and transmission shaft which are made by wire cutting. And the switch structure and flywheel are fabricated with polylactic acid (PLA) with the assistance of 3D printer (A8s, JGAURORA, P. R. China). The shell is made of acrylic panels.

The generator unit includes two parts: the rotor and the stator. Twelve copper electrodes with 100  $\mu\text{m}$  (thickness)  $\times$  40 mm (width)  $\times$  30 mm (length) are arranged on the inner wall of the stator. Six flexible blades are attached to a rotor. The flexible blades are FEP films with 100  $\mu\text{m}$  (thickness)  $\times$  40 mm (width)  $\times$  55 mm (length).

*Electrical Measurement:* A two-phase hybrid stepping motor (J-5718HBS401, Longshun, China) provides external incentive for MR-TENG, especially under the condition of wave water. An electrometer (6514, Keithley, USA) was used to collect the output signal of the prototype. And it was converted by a data acquisition system (PCI-6259, National Instruments, USA). Finally, the LabVIEW was applied to display and storage of data generated.

### Supporting Information

Supporting Information is available from the Wiley Online Library or from the author.

### Acknowledgements

M.Y., X.L., and G.Q. contributed equally to this work. The authors are grateful for the support received from the National Key R&D Project from the Minister of Science and Technology (2016YFA0202704), the Beijing Municipal Science and Technology Commission (Z171100002017017), and the National Natural Science Foundation of China (51775130).

### Conflict of Interest

The authors declare no conflict of interest.

## Keywords

controllable output performance, mechanical regulation, random excitation, triboelectric nanogenerators, wave energy harvesting

Received: February 18, 2020

Revised: March 20, 2020

Published online:

- 
- [1] Z. L. Wang, *ACS Nano* **2013**, *7*, 9533.
- [2] Z. L. Wang, W. Wu, *Angew. Chem., Int. Ed.* **2012**, *51*, 11700.
- [3] M. Asif, T. Muneer, *Renewable Sustainable Energy Rev.* **2007**, *11*, 1388.
- [4] M. Höök, X. Tang, *Energy Policy* **2013**, *52*, 797.
- [5] Q. Schiermeier, J. Tollefson, T. Scully, A. Witze, O. Morton, *Nature* **2008**, *454*, 816.
- [6] C. W. Marshall, *Nature* **1956**, *177*, 1050.
- [7] X. Wen, W. Q. Yang, Q. S. Jing, Z. L. Wang, *ACS Nano* **2014**, *8*, 7405.
- [8] Y. Yang, G. Zhu, H. Zhang, J. Chen, X. Zhong, Z. H. Lin, Y. J. Su, P. Bai, X. N. Wen, Z. L. Wang, *ACS Nano* **2013**, *7*, 9461.
- [9] Y. J. Ko, H. S. Kim, J. H. Jung, *J. Korean Phys. Soc.* **2017**, *71*, 679.
- [10] Q. Shi, H. Wang, H. Wu, C. Lee, *Nano Energy* **2017**, *40*, 203.
- [11] F. Fan, Z. Tian, Z. L. Wang, *Nano Energy* **2012**, *1*, 328.
- [12] D. Choi, S. Lee, S. M. Park, H. Cho, W. Hwang, D. S. Kim, *Nano Res.* **2015**, *8*, 2481.
- [13] S. B. Jeon, D. Kim, M. L. Seol, S. J. Park, Y. K. Choi, *Nano Energy* **2015**, *17*, 82.
- [14] S. Niu, S. Wang, Y. Liu, Y. S. Zhou, L. Lin, Y. Hu, K. C. Pradel, Z. L. Wang, *Energy Environ. Sci.* **2014**, *7*, 2339.
- [15] Z. Quan, C. B. Han, T. Jiang, Z. L. Wang, *Adv. Energy Mater.* **2016**, *6*, 1501799.
- [16] M. L. Seol, S. B. Jeon, J. W. Han, Y. K. Choi, *Nano Energy* **2017**, *31*, 233.
- [17] X. F. Wang, S. M. Niu, Y. J. Yin, Y. F. Z. You, Z. L. Wang, *Adv. Energy Mater.* **2015**, *5*, 1501467.
- [18] S. B. Lang, *Phys. Today* **2005**, *58*, 31.
- [19] S. Li, *Front. Optoelectron.* **2017**, *10*, 38.
- [20] X. S. Meng, H. Y. Li, G. Zhu, Z. L. Wang, *Nano Energy* **2015**, *12*, 606.
- [21] A. S. M. I. Uddin, G.-S. Chung, *Sens. Actuators, B* **2017**, *245*, 1.
- [22] H. M. Yang, W. L. Liu, Y. Xi, M. H. Lai, H. Y. Guo, G. L. Liu, M. F. Wang, T. Li, X. Ji, X. G. Li, *Nano Energy* **2018**, *47*, 539.
- [23] X. Y. Yang, S. Chan, L. Y. Wang, W. A. Daoud, *Nano Energy* **2018**, *44*, 388.
- [24] J. D. Zook, S. T. Liu, *J. Appl. Phys.* **1978**, *49*, 4604.
- [25] Y. Hu, J. Yang, Q. Jing, S. Niu, W. Wu, Z. L. Wang, *ACS Nano* **2013**, *7*, 10424.
- [26] C. Wu, P. Jiang, W. Li, H. Guo, J. Wang, J. Chen, M. R. Prausnitz, Z. L. Wang, *Adv. Funct. Mater.* **2020**, *30*, 1907378.
- [27] Y. Yang, H. Zhang, R. Liu, X. Wen, T.-C. Hou, Z. L. Wang, *Adv. Energy Mater.* **2013**, *3*, 1563.
- [28] Y. Yang, G. Zhu, H. Zhang, J. Chen, X. Zhong, Z.-H. Lin, Y. Su, P. Bai, X. Wen, Z. L. Wang, *ACS Nano* **2013**, *7*, 9461.
- [29] M. Y. Xu, T. C. Zhao, C. Wang, S. L. Zhang, Z. Li, X. X. Pan, Z. L. Wang, *ACS Nano* **2019**, *13*, 1932.
- [30] Z. L. Wang, *Nano Energy* **2019**, *68*, 104272.
- [31] C. Wu, A. C. Wang, W. Ding, H. Guo, Z. L. Wang, *Adv. Energy Mater.* **2019**, *9*, 1802906.
- [32] H. Zou, Y. Zhang, L. Guo, P. Wang, X. He, G. Dai, H. Zheng, C. Chen, A. C. Wang, C. Xu, Z. L. Wang, *Nat. Commun.* **2019**, *10*, 1427.
- [33] M. L. Seol, J. W. Han, D. I. Moon, K. J. Yoon, C. S. Hwang, M. Meyyappan, *Nano Energy* **2018**, *44*, 82.
- [34] K. Tao, H. Yi, Y. Yang, H. Chang, J. Wu, L. Tang, Z. Yang, N. Wang, L. Hu, Y. Fu, J. Miao, W. Yuan, *Nano Energy* **2020**, *67*, 104197.
- [35] W. Yang, Y. Wang, Y. Li, J. Wang, T. Cheng, Z. L. Wang, *Nano Energy* **2019**, *66*, 104104.
- [36] Y. Kim, J. Lee, J. Park, *IEEE/ASME Trans. Mechatronics* **2013**, *18*, 1839.